Bifurcations, stability, and dynamics of multiple matter-wave vortex states

S. Middelkamp,[1] P. G. Kevrekidis,[2] D. J. Frantzeskakis,[3] R. Carretero-González,[4,*] and P. Schmelcher[1]
[1]*Zentrum für Optische Quantentechnologien, Universität Hamburg, Luruper Chaussee 149, D-22761 Hamburg, Germany*
[2]*Department of Mathematics and Statistics, University of Massachusetts, Amherst, Massachusetts 01003-4515, USA*
[3]*Department of Physics, University of Athens, Panepistimiopolis, Zografos, Athens GR-15784, Greece*
[4]*Nonlinear Physics Group, Departamento de Física Aplicada I, Universidad de Sevilla, E-41012 Sevilla, Spain*
(Received 12 May 2010; published 30 July 2010)

In the present work, we offer a unifying perspective between the dark soliton stripe and the vortex multipole (dipole, tripole, aligned quadrupole, quintopole, etc.) states that emerge in the context of quasi-two-dimensional Bose-Einstein condensates. In particular, we illustrate that the multivortex states with the vortices aligned along the (former) dark soliton stripe sequentially bifurcate from the latter state in a supercritical pitchfork manner. Each additional bifurcation adds an extra mode to the dark soliton instability and an extra vortex to the configuration; moreover, the bifurcating states inherit the stability properties of the soliton prior to the bifurcation. The critical points of this bifurcation are computed analytically via a few-mode truncation of the system, which clearly showcases the symmetry-breaking nature of the corresponding bifurcation. We complement this small(-er) amplitude, few mode bifurcation picture, with a larger amplitude, particle-based description of the ensuing vortices. The latter enables us to characterize the equilibrium position of the vortices, as well as their intrinsic dynamics and anomalous modes, thus providing a qualitative description of the nonequilibrium multivortex dynamics.

DOI: 10.1103/PhysRevA.82.013646 PACS number(s): 03.75.Lm, 67.90.+z

I. INTRODUCTION

One of the most fundamental and thoroughly studied type of excitations in the realm of Bose-Einstein condensates (BECs) is the matter-wave vortex; see the reviews [1–6]. In two- (but also often in higher-) dimensional settings these structures are also of particular interest not only in nonlinear optics [7,8] (see also the reviews [9,10]) but also more broadly in nonlinear field theories in various branches of science [11]. Nevertheless, BECs represent a pristine setting where numerous features of the exciting nonlinear dynamics of single- and multicharge vortices, as well as of vortex crystals and vortex lattices, can be not only theoretically studied but also experimentally observed. More specifically, from the viewpoint of experiments, the first experimental observation of vortices [12] by means of a phase-imprinting method between two hyperfine spin states of a ^{87}Rb BEC [13] paved the way for a systematic investigation of their dynamical properties. Stirring the BECs [14] above a certain critical angular speed [15–17] led to the production of few vortices [17] and even of robust vortex lattices [18]. Other vortex-generation techniques were also used in experiments, including the breakup of the BEC superfluidity by dragging obstacles through the condensate [19], as well as nonlinear interference between condensate fragments [20]. In addition, apart from unit-charged vortices, higher-charged vortex structures were produced [21] and their dynamical (in-)stability was examined.

In the BEC context, a theme that has received somewhat lesser attention, chiefly from the theoretical point of view, is that of "crystals" or clusters consisting of small numbers of vortices. In an important earlier work [22], the emergence of vortex dipole states out of dark soliton stripes via a symmetry-breaking bifurcation was illustrated. Furthermore, in Refs. [23,24], more complicated states such as vortex dipoles, tripoles, and quadrupoles [23] were illustrated, and energetic arguments concerning their instability were provided; in particular, it was argued that all these states correspond to energy maxima. Later, in Ref. [24], a linear stability of these states led to the result that they are, in fact, unstable through different types of mechanisms (that we will discuss in more detail later in the article). A dynamical perspective, focusing especially on the vortex evolution and the vortex interactions, was adopted in Ref. [25]; note that in this work, the vortices were considered in the vicinity of the linear or weakly interacting limit. More recently, in Ref. [26], the bifurcation of the vortex dipole state from the dark soliton stripe was reproduced and a relevant explanation was attempted through a variational approximation; additionally, in the same work, the precessional dynamics of the vortex dipole near its equilibrium (as well as the potential for more complicated large-amplitude trajectories) was revealed. It should also be noted that similar vortex clusters have been considered in other settings, including toroidal traps as, e.g., in the earlier works of Refs. [27,28] as well as the more recent considerations of Ref. [29], rotating condensates with pinning sites of laser beams [30], or rotating anisotropic traps (which may enforce a linear arrangement of the vortices [31]).

At this point, it is also relevant to discuss the connection of vortex dipoles with the states out of which they were shown to emerge, namely the dark solitons (see the recent review [32]). The earlier experiments demonstrated the existence of these structures in BECs with repulsive interatomic interactions; the dark solitons were found to be unstable, exhibiting short lifetimes, mainly due to thermal [33,34] and dimensionality [35] effects. Regarding the latter, Ref. [35] reported the experimental observation of the onset of the transverse modulational instability of dark soliton stripes, as well as their concomitant

[*]On sabbatical leave from the Nonlinear Dynamical System Group [http://nlds.sdsu.edu], Department of Mathematics and Statistics, San Diego State University, San Diego, California 92182-7720, USA.

 ©2010 The American Physical Society

decay into vortex structures, in accordance to the theoretical predictions [36,37] and similar findings in nonlinear optics [9,38,39]. The transverse instability of dark solitons exhibiting radial symmetry [40] was also systematically studied [41,42]. Other theoretical works have investigated the possibility of avoiding the transverse instability of dark solitons, e.g., by using sufficiently tight traps [43,44], highly anisotropic traps [i.e., quasi one-dimensional (1D) traps], or narrow external potential sheets [45], that would enable the persistence of stable dark solitons [46]. From the viewpoint of experiments, the use of quasi-1D traps eventually allowed the recent experimental observation of robust, long-lived dark soliton states [47–50].

Motivated by these works, as well as by the very recent experimental observations of robust vortex dipoles [51,52] and of three-vortex states in Ref. [53], our aim in this work is to revisit this subject, providing a picture that (a) unifies the earlier findings and (b) connects them more firmly to the recent experiments. As far as the latter are concerned, in Ref. [51], vortex dipoles were produced by dragging a localized light beam with appropriate speed through the BEC, while in Ref. [52] they were distilled through the Kibble-Zurek mechanism [54] that was first experimentally reported for vortices in Ref. [55]. Note that in Ref. [52], near-equilibrium dynamics of the vortices was also observed, along with small amplitude motions of the dipole constituents, as well as large (distinct) amplitude, nearly decoupled precessional motions thereof. Furthermore, in Ref. [53], different types of three-vortex configurations were produced by applying an external quadrupolar magnetic field on the BEC. Among them, an aligned tripole configuration with a vortex of one topological charge straddling two other oppositely charged vortices, and an equilateral triangle of three same charge vortices were found to be prevalent within the experimental observations. Having in mind these findings, as well as the earlier results in this context, this work offers the following unifying perspectives in the context of quasi-two-dimensional (2D) BECs confined in harmonic, nonrotating traps. (i) We illustrate that the dimensionality-induced destabilization of the dark soliton leads, through a supercritical pitchfork bifurcation, to the formation of the vortex dipole. Further destabilizations of the dark soliton lead to the formation of the stationary tripole, aligned quadrupole, quintopole, and so on. (ii) We clarify the relevant nature of such supercritical pitchfork bifurcations and illustrate their symmetry breaking character, through a few mode expansion that enables an *analytical* prediction of the bifurcation point of the emergence of these states. (iii) We systematically study the stability of each of these states by elucidating their complete linearization spectrum, anomalous modes, and imaginary, as well as complex eigenfrequency instabilities; we also showcase the connections of this spectrum with the bifurcation picture presented through general principles of bifurcation theory. (iv) We formulate a complementary physical picture, which considers the vortices as individual particles precessing within the parabolic trap and interacting with each other through the modification of each other's local velocity field. This picture allows us to predict not only the equilibrium position of the vortices, e.g., in a dipole setting, but also (and perhaps even more importantly) the near-equilibrium dynamics, e.g., the anomalous modes of the vortex pair and the epicyclic motions associated with the nontrivial one among these modes. (v) Finally, we use this particle picture as a guide toward some of the more complex vortex dynamics which we corroborate through direct numerical simulations; clearly, however, the latter is a rich area that merits additional investigation.

Our presentation will be structured as follows. In Sec. II, we present our model and briefly review the dynamics of a single unit-charge vortex. In Sec. III, we present our theoretical analysis for the few-mode bifurcation picture, which is particularly relevant close to the linear limit. We complement this with a large-amplitude perspective, whereby dynamical equations for two or more isolated vortices are considered, and their static, stability, and dynamical implications are examined. Subsequently, in Sec. IV, we embark on a detailed numerical bifurcation study of the states emerging from the dark soliton stripe (as well as of a few that do not arise from it). In Sec. V, we corroborate some of the near-equilibrium static (linearization) picture with direct numerical simulations; we also consider a few more exotic dynamical implications of the original model [and of its underlying ordinary differential equation (ODE) counterpart]. Finally, in Sec. VI, we summarize and present our conclusions, as well as speculate on some interesting potential directions for future studies.

II. MODEL AND BACKGROUND

A. The 2D mean-field model and BdG analysis

We consider a quasi-2D (alias "disk-shaped") condensate confined in a highly anisotropic trap with frequencies ω_z and $\omega_\perp$ along the longitudinal and transverse directions, respectively. In the case $\omega_\perp \ll \omega_z$ and $\mu \ll \hbar\omega_z$ (where μ is the chemical potential), and for sufficiently low temperatures, the transverse part $u(x,y,t)$ of the macroscopic BEC wave function obeys the following $(2+1)$-dimensional Gross-Pitaevskii equation (GPE) [6]:

$$i\hbar\partial_t u = \left[-\frac{\hbar^2}{2m}\nabla_\perp^2 + V(r) + g_{2D}|u|^2 - \mu\right]u, \qquad (1)$$

where $r^2 = x^2 + y^2$, $\nabla_\perp^2 = \partial_x^2 + \partial_y^2$ is the transverse Laplacian, while the potential is given by $V(r) = (1/2)m\omega_\perp^2 r^2$ (where m is the atomic mass). The effective 2D nonlinearity strength is given by $g_{2D} = g_{3D}/\sqrt{2\pi}a_z = 2\sqrt{2\pi}aa_z\hbar\omega_z$, with $g_{3D} = 4\pi\hbar^2 a/m$, a and $a_z = \sqrt{\hbar/m\omega_z}$ denoting, respectively, the three-dimensional (3D) interaction strength, the s-wave scattering length, and the longitudinal harmonic oscillator length. Equation (1) can be expressed in the following dimensionless form,

$$i\,\partial_t u = \left[-\tfrac{1}{2}\nabla^2 + V(r) + |u|^2 - \mu\right]u, \qquad (2)$$

where the density $|u|^2$, length, time, and energy are, respectively, measured in units of $(2\sqrt{2\pi}aa_z)^{-1}$, a_z, ω_z^{-1}, and $\hbar\omega_z$. Finally, the harmonic potential is now given by $V(r) = (1/2)\Omega^2 r^2$, with $\Omega = \omega_\perp/\omega_z$. From here, all equations will be presented in dimensionless units for simplicity.

In the following, we will analyze the existence and linear stability of the nonlinear modes of Eq. (2). Note that numerically the relevant nonlinear states will be identified as a function of the chemical potential μ by means of a fixed point (Newton iteration) scheme over a rectangular

two-dimensional grid with suitably small spacing.[1] Linear stability will be explored by means of the Bogoliubov-de Gennes (BdG) analysis. The latter, involves the derivation of the BdG equations, which stem from a linearization of the GPE Eq. (2) around the stationary solution $u_0(x,y)$ by using the ansatz

$$u = u_0(x,y) + [a(x,y)e^{i\omega t} + b^*(x,y)e^{-i\omega^* t}], \tag{3}$$

where $*$ denotes complex conjugate. The solution of the ensuing BdG eigenvalue problem yields the eigenfunctions $\{a(x,y),b(x,y)\}$ and eigenfrequencies ω. As concerns the latter, we note that due to the Hamiltonian nature of the system, if ω is an eigenfrequency of the Bogoliubov spectrum, so are $-\omega$, ω^*, and $-\omega^*$. Note that a linearly stable configuration is tantamount to $\mathrm{Im}(\omega) = 0$, i.e., all eigenfrequencies being real.

An important quantity resulting from the BdG analysis is the amount of energy carried by the normal mode with eigenfrequency ω, namely,

$$E = \int dxdy(|a|^2 - |b|^2)\omega. \tag{4}$$

The sign of this quantity, known as the *Krein sign* [56], is a topological property of each eigenmode. For one of the eigenvalues of each double pair this sign is negative. The corresponding mode is called the *anomalous mode* [1], the *negative-energy mode* [57], or the mode with the *negative Krein signature* [56]. If such a mode becomes resonant with a mode with a positive Krein signature, then, typically, complex frequencies appear in the excitation spectrum, i.e., a dynamical instability arises [56].

B. Vortex states

Vortices are characterized by their nonzero topological charge S whereby the phase of the wave function has a phase jump of $2\pi S$ along a closed contour surrounding the core of the vortex. Exact analytical vortex-state solutions of Eq. (1) are not available. Nevertheless, in the noninteracting limit, a linear state analogous to the vortex consists of a superposition of the energetically degenerate first excited states (see in the following). Then, in the (nonlinear) case where interatomic interactions are present, a vortex state can be found by performing a continuation from such a linear state.

Following the recent work [58], the equations of motion for the vortex center (x_v, y_v) take the form (for small displacements of the vortex from the center of the trap),

$$\dot{x}_v = -S\frac{\Omega^2}{2\mu}\ln\left(A\frac{\mu}{\Omega}\right)y_v, \tag{5}$$

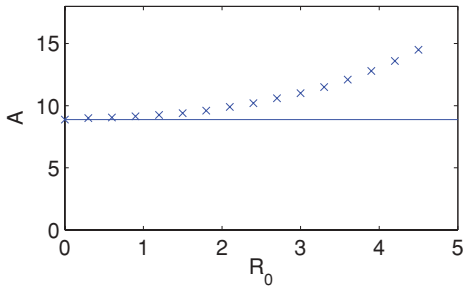

FIG. 1. Dependence of the numerical factor A [see Eqs. (5) and (6)] on the initial displacement R_0 of the vortex from the center of the trap, for $\mu = 3$.

$$\dot{y}_v = S\frac{\Omega^2}{2\mu}\ln\left(A\frac{\mu}{\Omega}\right)x_v, \tag{6}$$

where S denotes the topological charge (alias "vorticity") and A is an appropriate numerical factor, taking the value $A \approx 8.88 \approx 2\sqrt{2}\pi$. Equations (5) and (6) suggest a precession of the vortex in the harmonic trap with a frequency

$$\omega_{\mathrm{pr}} = \frac{\Omega^2}{2\mu}\ln\left(A\frac{\mu}{\Omega}\right). \tag{7}$$

Naturally, the amplitude of the precession is fixed and fully determined by the initial distance $R_0 = \sqrt{x_0^2 + y_0^2}$ of the vortex location from the trap center. While these results are in excellent agreement with numerical computations for small R_0, it is worth investigating the dependence of the precession frequency on R_0 for intermediate and/or large radii. In that regard, Fig. 1, which shows the dependence of A on R_0 (for $\mu = 3$), suggests that the value of the numerical factor A changes for large initial displacements: in fact, up to $R_0 < 1.5$, the value $A \approx 2\sqrt{2}\pi$ (corresponding to infinitesimally small displacements) yields a good approximation, while for larger displacements R_0, the value of A is increased, indicating the faster rotation of the vortices away from the condensate center.

Having discussed the dynamics of a single vortex in the trap, let us now consider the vortex-vortex interaction. Based on the analogy with fluid vortices [59], it has been argued that the superfluid vortices considered herein have similar interaction laws and corresponding kinematic equations. In particular, on a homogeneous background, and for large distances of the vortices compared to the size of the vortex core, the kinematic equations for vortices with centers (x_m, y_m) and (x_n, y_n) take the form [5,60]

$$\dot{x}_m = -BS_n\frac{y_m - y_n}{2\rho^2}, \tag{8}$$

$$\dot{y}_m = BS_n\frac{x_m - x_n}{2\rho^2}, \tag{9}$$

with $\rho = \sqrt{(x_m - x_n)^2 + (y_m - y_n)^2}$, $S_n = \pm 1$ the vorticity of the vortex n and an appropriate numerical factor B; in the case of the homogeneous condensate, the latter takes the value $B \approx 1.95$.

[1] We opt to use the chemical potential as a relevant parameter here, rather than the nonlinearity strength. This will have two significant advantages. On the one hand, it will render more transparent the connections of the nonlinear states to the linear limit eigenstates of the problem. On the other hand, it will enable us to exploit the two-mode theory of nonlinear states arising from linear states (and the symmetry-breaking bifurcations from these); see, e.g., G. Theocharis, P. G. Kevrekidis, D. J. Frantzeskakis, and P. Schmelcher, Phys. Rev. A **74**, 056608 (2006).

III. THEORETICAL ANALYSIS

A. Dark soliton stripe bifurcation picture

Let us now proceed by investigating the existence and possible bifurcations of the lowest macroscopically excited states of Eq. (2). In the following, we fix the trap strength using $\Omega = 0.2$. In the noninteracting (linear) case, the Hamiltonian describing the stationary states can be written as $\hat{H} = \hat{H}_x + \hat{H}_y$, with $\hat{H}_x$ and $\hat{H}_y$ being the Hamiltonian of a single particle in a harmonic trap oriented along the x and y directions, respectively. Therefore, the linear states factorize as well and can be written as $\Psi_{nm}(x,y) = \psi_n(x)\psi_m(y)$ with $\psi_n(x)$ and $\psi_m(y)$ being the states associated to the nth and mth eigenvalue of $\hat{H}_x$ and $\hat{H}_y$, respectively. The resulting states $\Psi_{nm}(x,y)$ with energy $\mu = (n+m+1)\Omega$ denote the eigenstates of the linear limit. Due to the rotational symmetry of the problem, one can rotate any solution around the center of the trap obtaining another solution. Hence, when we consider in the following a solution with a distinct symmetry direction one needs to have in mind that the direction may be chosen arbitrarily.

The top panel of Fig. 2 shows the number of atoms N as a function of the chemical potential for different branches of possible solutions. The bottom panel in this figure shows, for better clarity of exposition, the atom difference $\Delta N = N - N_{\rm ds}$ between the atom number N of a particular branch and the atom number $N_{\rm ds}$ for the dark soliton branch. We have not shown the branch of the ground state starting at $\mu = \Omega = 0.2$ from the linear limit, as the stable ground state of the system will not be relevant in our discussion hereafter.

The first branch, with the largest atom number (among the ones considered therein) for fixed chemical potential, is the single-vortex (sv) state located at the center of the trap. It is well established that this solution is dynamically stable [1–6], despite of the fact that it possesses an anomalous mode in its excitation spectrum (the eigenfrequency of the anomalous mode coincides with the small amplitude precession frequency; see, e.g., Ref. [58]). In the linear limit, this state is given by $\Psi_{\rm sv}(x,y) = \psi_1(x)\psi_0(y) + i\psi_0(x)\psi_1(y)$. Therefore, it is "initialized" at an energy of $\mu = 2\Omega$. For increasing chemical potential the atom number increases monotonically. Furthermore, no other states bifurcate from this one (given its existence properties and its absence of stability changes).

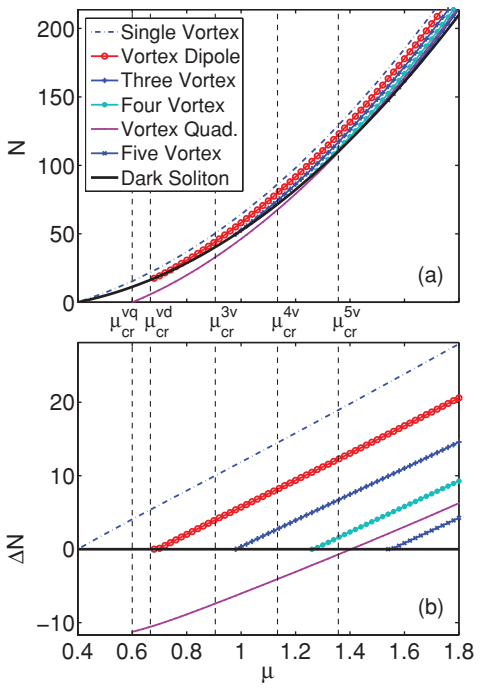

FIG. 2. (Color online) (Top) Number of atoms as a function of the chemical potential for the different states for $\Omega = 0.2$. (Bottom) Corresponding number of atom difference between the different branches and the dark soliton stripe branch.

The second (and most critical for our discussion herein) branch starts from $\mu = 2\Omega$ in the linear limit as well. The wave function of this branch is given in the linear limit by $\Psi_{\rm ds}(x,y) = \Psi_{10}(x,y) = \psi_1(x)\psi_0(y)$ (without loss of generality we assumed the relevant stripe to be oriented along the y axis). This state, which has a density minimum along the y axis and a phase jump across this minimum, is precisely the dark soliton (ds) stripe with the line symmetry that characterizes such a 2D generalization of the 1D dark soliton.

The essence of our discussion lies in the (symmetry-breaking) bifurcations arising from the dark soliton stripe solution. In particular, in the case of $\Omega = 0.2$ considered in Fig. 2, and for $\mu \approx 0.68$, the vortex dipole state emerges. This is clearly a supercritical pitchfork bifurcation, as there are two potential installments of such a dipole with opposite, between them, relative positions of their $S = 1$ and $S = -1$ vortex constituents. The location of this bifurcation is sufficiently close to the linear limit so that it can be predicted by using a Galerkin-type approach [61] (see also Refs. [62,63] for a general discussion). The dark soliton state is given, close to the linear limit, by $\Psi_{\rm ds}(x,y) = \psi_1(x)\psi_0(y)$. The vortex dipole (vd) state occurs due to an admixture of the $\Psi_{02}(x,y) = \psi_0(x)\psi_2(y)$ state to $\Psi_{\rm ds}$, but importantly with a phase difference of $\pi/2$ with respect to the $\Psi_{\rm ds}$. Hence, the bifurcation theory developed in Ref. [61] can be directly applied but with the crucial difference of the relative phase of the symmetry-breaking admixing state (with respect to the original state) of $\phi = \pi/2$. In that case, one can repeat the calculations of Ref. [61] [cf. Eq. (10) therein] to obtain the relevant bifurcation point as:

$$N_{\rm cr} = \frac{\omega_{10} - \omega_{02}}{I - I_0}, \tag{10}$$

where $\omega_{10,02}$ are the eigenvalues corresponding to the states $\Psi_{10}(x,y)$ and $\Psi_{02}(x,y)$, $I_0 = \int \Psi_{10}^4 dx\,dy$, and $I = \int \Psi_{10}^2 \Psi_{02}^2 dx\,dy$. One can also determine the critical chemical potential at which the symmetry breaking is expected to occur, namely $\mu_{\rm cr} = \omega_{10} + I_0 N_{\rm cr}$ [61]; for these parameter values, this leads to $\mu_{\rm cr}^{\rm vd} = \frac{10}{3}\Omega$ ($= 2/3$ for $\Omega = 0.2$, see second vertical thin dashed line in the case shown in Fig. 2), which is in excellent agreement with our numerical findings.

For larger chemical potential, at $\mu \approx 0.98$, another branch bifurcates from the dark soliton branch. The wave functions of this branch contain three vortices (3v) oriented along a line with adjacent vortices having opposite vorticity. It is remarkable that although this bifurcation happens quite far from the linear limit, one can still understand it through the same supercritical pitchfork (symmetry-breaking) theoretical framework. In particular, what is happening in this case is

that the Ψ_{03} state is providing the "admixture" element to the "pure" dark soliton stripe state. In light of that, the analysis presented here [and Eq. (10)] still holds but now $\omega_{02} \to \omega_{03} = 3\Omega$ and $I = \int \Psi_{10}^2 \Psi_{03}^2 dx\, dy$. Repeating the same calculation as before, one finds $\mu_{\rm cr}^{\rm 3v} = 86\Omega/19$ (which in this case is $\approx$0.91, see the third vertical thin dashed line in Fig. 2, in reasonable agreement with the numerical result just provided). Given the substantial departure from the linear limit and the nonlinear deformation of the dark soliton stripe (still represented in this phenomenology by its linear limit of Ψ_{10}), this slight discrepancy can be well understood. Furthermore, the symmetry-breaking, supercritical pitchfork nature of the bifurcation is again evident since two installments of the same "vortex tripole" (as it will be called in the following) branch may emerge, one with two $S = 1$ vortices and an $S = -1$ centrally separating them and one with two $S = -1$ vortices with an $S = 1$ between them.

At $\mu \approx 1.26$ a four-vortex (4v) state (an aligned quadrupole), with the vortices oriented along a line, bifurcates from the dark soliton state. At this point, the sequence of symmetry breaking events is clear: now the Ψ_{04} is offering the $\pi/2$ out of phase admixture leading to a critical point through the same procedure and the corresponding reformulation of the previous constants of $\mu_{\rm cr}^{\rm 4v} = 890\Omega/157$; in connection to the $\Omega = 0.2$ case of Fig. 2, we find $\mu_{\rm cr}^{\rm 4v} \approx 1.13$ (see fourth vertical thin dashed line), with the slight progressive degradation of the critical point attributable again to the further departure from the linear limit. In this case also, the vortex parity variation of $S \to -S$ for such a four-vortex line configuration whose adjacent vortices possess opposite charges yields the two bifurcating branches associated with this critical point.

However, we should note in passing here that a state with four vortices exists even in the linear limit as is shown by the branch starting at $\mu = 3\Omega$ in the linear limit: this represents a four-vortex state, with vortices located at the vertices of a square, i.e., a vortex quadrupole (vq). This is among the states previously considered in Ref. [23,24], as well as independently proposed as a member of a larger class of so-called vortex necklace states in Ref. [64]. At the linear limit, this state can be represented, e.g., as $\Psi_{\rm vq}(x,y) = \psi_2(x)\psi_0(y) + i\psi_0(x)\psi_2(y)$ and emerges from the linear limit at $\mu_{\rm cr}^{\rm vq} = 3\Omega$ (= 0.6 in the case of Fig. 2, cf. first vertical thin dashed line in the figure). With increasing chemical potential the number of atoms of the state monotonically increases. At $\mu \approx 1.4$ this branch crosses the branch representing the dark soliton stripe. However, it is important to note that due to the structural disparity of those states, the crossing of the number of atoms (contrary to the previous cases considered here) does *not* constitute a bifurcation and therefore does not lead to any stability change.

Nevertheless, at higher values of μ (e.g., for $\mu \approx 1.54$ in the case of $\Omega = 0.2$ of Fig. 2), a five-vortex (5v) state (a vortex quintopole) bifurcates from the dark soliton stripe. Once again, the vortices are oriented along a line and adjacent vortices have opposite vorticities. Furthermore, the bifurcation shares the standard supercritical pitchfork character of the earlier ones, and its characterization through analytical tools presented here reveals a critical point at $\mu_{\rm cr}^{\rm 5v} = 726\Omega/107$ (which, for $\Omega = 0.2$, leads to $\mu_{\rm cr}^{\rm 5v} \approx 1.36$, see last vertical thin dashed line in Fig. 2). According to our results here, the structural progression of these symmetry-breaking events is clear and we will not proceed to characterize higher ones among them, especially given the dynamical instability of the ones beyond the vortex dipole state (that will be discussed in more detail in the following).

However, let us add a short note about the physical intuition of the general picture. What is happening in the present setting is that there exists a sequence of supercritical pitchfork bifurcations in which the Ψ_{10} gets mixed progressively with each of the Ψ_{0m} modes. In so doing, the m-fold symmetry of the latter breaks the line symmetry of the former. In addition, the $\pi/2$ relative phase between them introduces a picture which locally at each perpendicular intersection of the m nodal lines of the latter with the nodal line of the former resembles a $\Psi_{10} \pm i\Psi_{01}$ (with the pluses alternating with the minuses due to the field structure of the Ψ_{0m}). As a result, at each of these nodal line intersections, vortices with alternating (between adjacent ones) charges emerge, progressively formulating the dipole, tripole, aligned quadrupole, quintopole, and so on.

B. Vortex particle complementary picture

This discussion and bifurcation picture is especially relevant close to the point of emergence of these multivortex solution branches. A complementary aspect of our description concerns the case (for larger chemical potentials) where the vortices are well separated, individual interacting entities which can be regarded as interacting particles subject to the precessional effect due to the parabolic confinement. In that picture, it is relevant to develop (kinematic) equations of motion characterizing the vortex dynamical evolution, as well as their potential equilibrium positions and their near-equilibrium behavior, similarly to what was done, e.g., for characterizing the oscillations and interactions of dark solitons in quasi-one-dimensional settings in Ref. [49] (see also Ref. [65]). In that light, we combine Eqs. (5) and (6), describing the interaction of the background density of a condensate in a trap with each single vortex, and Eqs. (8) and (9) describing the interaction of (any pair of) two vortices on a homogeneous background, to provide the total contribution to the superfluid local velocity at the vortex location. This way, the vortex motion can be described as follows:

$$\dot{x}_m = -S_m \omega_{\rm pr} y_m - B S_n \frac{y_m - y_n}{2\rho_{mn}^2}, \tag{11}$$

$$\dot{y}_m = S_m \omega_{\rm pr} x_m + B S_n \frac{x_m - x_n}{2\rho_{mn}^2}. \tag{12}$$

It is worth noticing that although these equations refer to the case of two vortices, indexed by m and n, the relevant generalization to an *arbitrary* number of (precessing and interacting) vortices is imminently evident through the conversion of the second term in the right-hand side of Eqs. (11) and (12) into a sum over all $n \neq m$.

By focusing on the two-vortex setting for definiteness, our description yields a number of interesting conclusions. For $S_1 = -S_2 = 1$ the equations possess fixed points at

$$x_1 = x_2 = 0, \tag{13}$$

$$y_1 = -y_2 = \sqrt{\frac{B}{4\omega_{\rm pr}}}. \tag{14}$$

These are anticipated to be the equilibrium locations of the vortices within the vortex dipole. Furthermore, the linearization of the dynamical equations (11) and (12) around these equilibrium points offers insight into the fate of small perturbations around these steady-state locations. Part of the special appeal of this analysis is that it can provide *explicit, analytical* predictions for the *internal modes* of the vortex system. These are in fact, precisely, the anomalous modes of negative Krein signature or the unstable imaginary eigenfrequency modes pertaining to this non-ground-state type of structure, as we will illustrate in our numerical computations of the full system in the following; see also the corresponding discussion for a single vortex in Ref. [58] and for the quasi-1D analog of this picture in the dark soliton setting in Refs. [49,65]. The Jacobian matrix of the linearization around the equilibrium vortex dipole location offers the following insights. One of the vortex dipole linearization modes has a vanishing frequency, i.e., a pair of eigenfrequencies at $\omega = 0$. This is natural to expect: this frequency pair merely corresponds to the neutral direction associated with the "rotational freedom" of the vortex dipole pair, i.e., the ability to equivalently locate it at any pair of antidiametric points located at a distance given by Eq. (14) from the trap center. The other nonvanishing pair of linearization eigenmodes (of this 4×4 system) corresponds to a frequency:

$$\omega_{\rm pr}^{\rm vd} = \pm\sqrt{2}\omega_{\rm pr}. \tag{15}$$

This frequency characterizes the precessional motion of the vortex pair around this equilibrium position which can be naturally thought of as an "epicyclic" counter-rotation of the oppositely charged vortices. We now turn to the examination of these analytical findings by applying numerical existence and stability tools.

IV. SOLITON AND VORTEX STATES AND THEIR STABILITY

A. The single-vortex state

The single-vortex state has already been discussed in several works. We briefly mention this state for reasons of completeness and for comparison to the multivortex states. This structure exists for $\mu > 2\Omega$. The contour plots of the density (left) and its 2π winding phase (right) are shown in the upper panels of Fig. 3. Naturally, its equilibrium position is at the center of the trap (otherwise it would precess). The bottom panel shows the eigenfrequencies ω of the Bogoliubov spectrum as a function of the chemical potential μ. All eigenfrequencies are real denoting that the state is dynamically stable. However, one of the modes has negative energy, indicating that the state is energetically unstable. The negative-energy mode bifurcates in the linear limit from the dipole (or Kohn) mode, which has a constant magnitude equal to the trap frequency (in this case, $\Omega = 0.2$). As μ increases, the frequency of the negative-energy mode decreases, thus becoming the lowest excitation frequency of the system. The frequency of the negative-energy mode coincides with the precession frequency of the vortex around the center of the trap. The dash-dotted line indicates the precession frequency predicted by Eq. (7) with $A = 2\sqrt{2}\pi$. For large chemical potentials, the prediction of Eq. (7) agrees very well with our numerical findings. Furthermore, for small values of μ, one mode departs linearly from zero (due to the phase-induced breaking of the radial symmetry). The corresponding analytical prediction is given by the dashed line with the functional form $\omega = \mu - 2\Omega$ [58]. The sole remaining pair of zero eigenfrequencies is associated to the atom number conservation and the gauge invariance of the underlying model.

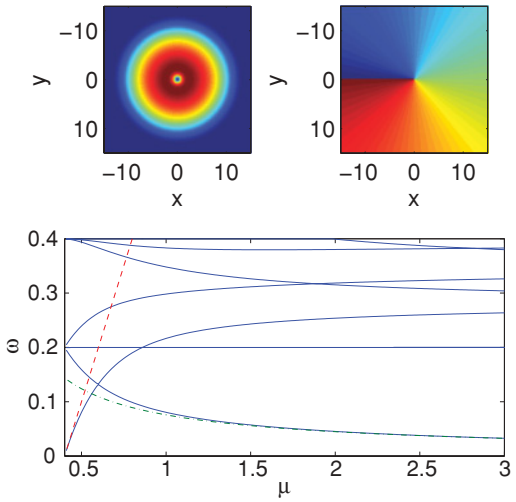

FIG. 3. (Color online) The single-vortex state for a trap of strength $\Omega = 0.2$. The top panels show contour plots of the density (left) and phase (right) of the wave function for $\mu = 3$, while the bottom panel shows the eigenfrequencies ω of the Bogoliubov spectrum as a function of the chemical potential μ. Theoretical predictions are given by the dashed line $\omega = \mu - 2\Omega$ and the dashed dotted line $\omega = \omega_{\rm pr}$, see Eq. (7). Note that, in the color online version, within the upper left panel, blue denotes zero and red maximal density. Similarly, in the upper right panel blue to red denotes a phase going from 0 to 2π.

B. The dark soliton state

The top panel of Fig. 4 shows contour plots of the density and phase of the dark soliton stripe for $\mu = 3$. The density has a minimum along the y axis associated with a π phase jump, characteristic of dark solitons. The dark soliton state exists for $\mu > 0.4$. The bottom panel shows the real and imaginary parts of the eigenvalues of the BdG spectrum as a function of the chemical potential. The real parts correspond to oscillation frequencies, whereas the imaginary parts imply dynamical instabilities. We note in passing that at some places some level crossings are observed (accompanied by mergers, e.g., for $\mu \in [1.1,1.3]$ of the real parts of the corresponding eigenfrequencies). These correspond to collisions of eigenmodes with opposite Krein signatures and lead to complex eigenfrequency quartets. However, because these only happen for small parametric regimes and the instabilities they induce are far weaker than the ones associated with purely imaginary eigenfrequencies (in fact, they appear as only "small bumps" and are at least an order of magnitude weaker than the principal instabilities in the bottom panel of Fig. 4), they will not be considered further hereafter.

Let us at first investigate the real part of the eigenfrequencies. The mode at $\omega = \Omega$ is twofold degenerate and corresponds to the dipolar mode which describes the oscillation of

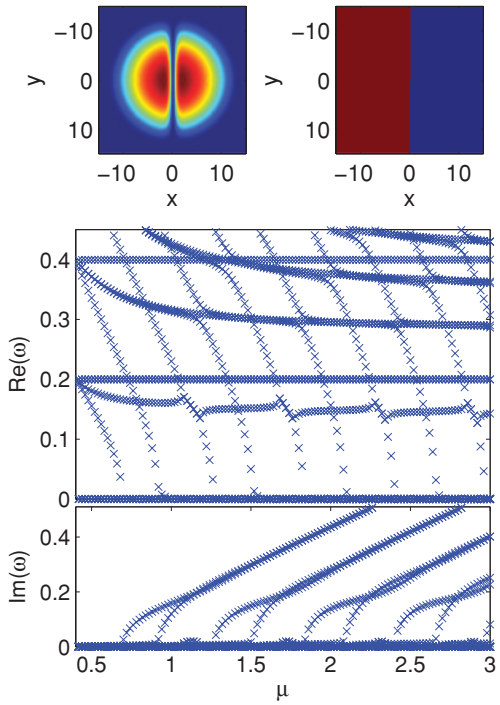

FIG. 4. (Color online) The dark soliton state for a trap strength $\Omega = 0.2$. The top panels show contour plots of the density (left) and phase (right) of the wave function for $\mu = 3$, while the bottom panel shows the eigenfrequency ω of the BdG spectrum as a function of the chemical potential μ.

the whole condensate with the trap frequency. The degeneracy occurs due to the symmetry of the trap, i.e., the trap frequencies in the x and y directions are equal. From this mode bifurcate two modes. The mode with smaller magnitude decreases to zero and becomes imaginary leading to a dynamical instability and the symmetry-breaking bifurcation discussed previously. The vanishing of the relevant eigenfrequency denotes the point of bifurcation of the vortex dipole from the dark soliton stripe (cf. Fig. 2). The other mode bifurcating from $\omega = \Omega$ has a negative energy or negative Krein signature. This mode looks similar to the mode of a dark soliton in a 1D condensate. In the latter setting, this mode is the only one with a smaller magnitude than the dipolar mode. It bifurcates from the dipolar mode and decreases with increasing chemical potential up to a threshold in the Thomas-Fermi limit of large chemical potentials. The general behavior of this mode is similar. However in the 2D case there exist other modes that may acquire a smaller real part than the dipolar modes. These modes bifurcate at the linear limit from $\omega = n\Omega$ (one per multiple of the trap frequency) and, upon decrease of their magnitude, they eventually cross zero and become imaginary leading to additional instabilities. When the negative-energy mode collides with these modes, it may form a band of oscillatory instability manifested in the quartet of complex eigenvalues, e.g., for $1.1 < \mu < 1.2$ (see also the previous discussion).

Every time one of these decreasing modes crosses zero, another one of the bifurcations discussed previously will arise. At the critical point of the bifurcation, the kernel of the dark soliton stripe linearization is augmented and becomes four (instead of two) dimensional. The additional pair of vanishing eigenfrequencies is associated with a rotational freedom that is, in turn, inherited by the resulting multivortex state. It is important to also mention here that given the supercritical pitchfork nature of the bifurcation, the novel emerging state (at *each* step of this bifurcation sequence) inherits the linear stability properties of its dark soliton stripe ancestor just before the bifurcation. In view of that, we have a clear roadmap of what to expect of the multivortex states' stability. In particular, the vortex dipole emerging out of the stable dark soliton stripe should itself be neutrally stable at least close to the bifurcation point. On the contrary, the vortex tripole, aligned quadrupole, quintopole, etc., should, respectively, inherit the one-, two-, three-, etc., respectively, unstable eigendirections of the dark soliton stripe at the critical parameter point of their bifurcation. We should note in passing here that changing the aspect ratio of the trap leads to a shift of the point where the individual modes of the spectrum cross zero and may, thus, be used to induce a stabilization of the dark soliton stripe. Eventually, the dark soliton becomes stable for quasi-1D traps [43,44,46].

It is interesting to parallel these results with those of Ref. [46], which also considered the destabilization of the dark soliton stripe, although in a waveguidelike trap geometry and through a fully numerical approach. The authors of Ref. [46] recognized the progressive destabilization steps of the dark soliton stripe as they augmented the transverse direction width in their geometry. However, they attributed the instabilities to single- or multivortex *decay* indicating that the multivortex patterns observed "are by no means stationary but rather form transient states" [46]. We believe that this picture strongly supports the emergence of stationary bifurcating structures of this multivortex type.

C. The vortex dipole state

We now turn to the first by-product of this bifurcation picture, namely the vortex dipole, which is shown in Fig. 5. The top panels of the figure show the contour plots of the density and phase of this coherent structure. The middle panel of Fig. 5 shows the dependence of the position of the vortices on the chemical potential for $\Omega = 0.1$, $\Omega = 0.15$, and $\Omega = 0.2$ (curves from top to bottom). The lines denote the corresponding prediction by the system of ordinary differential equations (ODEs) for the vortex centers through Eq. (14) for $A = 2\sqrt{2}\pi$ and $B = 1.35$. The ODE prediction agrees very well with the results of the full model. The bottom panel shows the real and imaginary part of the eigenfrequencies of the Bogoliubov spectrum as a function of the chemical potential for $\mu > 0.68$ (where the dipole state exists).

Examining in more detail the spectrum of this vortex dipole, we find the following. At $\omega = \Omega$, there exists again the twofold degenerate dipolar modes which are associated with the oscillation of the whole condensate in the x and y directions with the trap frequency. From these modes, there bifurcates toward lower frequencies a negative-energy mode, similar to the case of a single vortex. However, in this case, the negative-energy mode collides with the mode departing from zero and forms a band of complex eigenfrequencies associated with oscillatory instabilities. This is the *sole* (see also the discussion to follow below) and predominant, albeit quite weak, instability of the vortex dipole state. For larger chemical

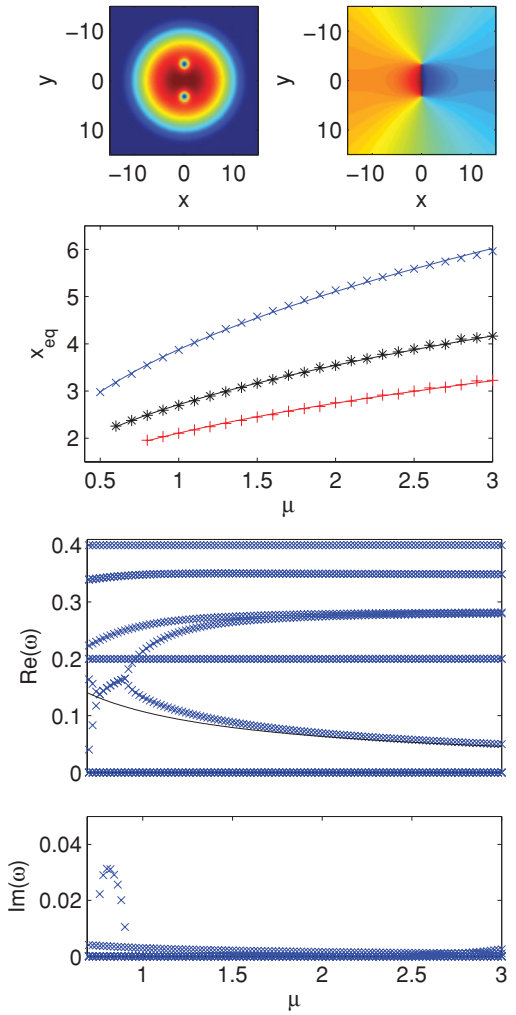

FIG. 5. (Color online) The vortex dipole state for a trap strength $\Omega = 0.2$. The top panels show contour plots of the density (left) and phase (right) of the wave function for $\mu = 3$. The middle panel shows the dependence of the position of the vortices on the chemical potential for $\Omega = 0.1$, $\Omega = 0.15$, and $\Omega = 0.2$ (curves from top to bottom). The lines indicate the predictions of the ODE with $A = 2\sqrt{2}\pi$, $B = 1.35$. The bottom panels show the real and imaginary parts of the eigenfrequencies ω of the BdG spectrum as a function of the chemical potential μ. The thin solid line shows the analytical prediction $\omega_{\rm pr}^{\rm vd} = \sqrt{2}\omega_{\rm pr}$.

potentials this degeneracy is lifted and the negative-energy mode behaves similarly to the case of the single vortex. However, in the vortex dipole case, the eigenfrequency of this mode for sufficiently large chemical potentials is very accurately predicted by Eq. (15), i.e., it is given by $\omega_{\rm pr}^{\rm vd} = \pm\sqrt{2}\omega_{\rm pr}$ and directly reflects the epicyclic counter-rotation of the two vortices around their equilibrium location. The spectrum has two pairs of zero modes associated with the gauge invariance of the model, as well as with the rotational invariance of the dipole location (within the radially symmetric trap). Notice that for the latter mode radial symmetry is crucial and the corresponding eigenfrequency gets shifted in the presence of planar anisotropy i.e., for $\omega_y \neq \omega_x$. To be more precise the mode becomes imaginary thereby destabilizing the system, if the trap strength is increased in the direction of the dipole. The magnitude of the imaginary mode increases with the anisotropy of the trap. On the other hand, if the trap strength is increased along the axis perpendicular to the dipole axis, then the relevant eigenfrequency becomes real and no instability arises.

It is worthwhile to place these results, and more generally the stability of the vortex dipole state, in the context of earlier works that had predicted such a structure. The original prediction of Ref. [22] cited the vortex dipoles as "extremely robust" but only employed direct integration methods (under noisy perturbations); hence, while suggestive, the findings of Ref. [22] could not preclude a potential instability (or trace its parametric regime). The subsequent investigation of Ref. [23] seemed to suggest the opposite, namely that the dipole was, in fact, unstable not only because of its constituting an energy maximum but also due to a number of (tabulated) values suggesting the presence of nonreal eigenfrequencies. This was more systematically considered in Ref. [24], which offered the imaginary parts of the relevant eigenfrequencies indicating two types of instabilities, a universal weak one (for all chemical potentials) and a stronger one for a narrow parametric regime. For the former, it was indicated that, as a result of its manifestation, the vortex dipole appears to remain intact through rotation and it was argued that it can be thought of as structurally stable, although dynamically unstable. These results are worthy of a close inspection and comparison with the bottom panel of Fig. 5. In fact, there, we also observe an extremely weak (of the order of 10^{-3} or smaller) but apparently systematically occurring (for all μ's) unstable eigenmode of imaginary eigenfrequency. However, based on physical grounds, we argue that this mode is likely to be a manifestation of the accuracy of the numerical eigenvalue computations involved herein (cf. Ref. [66]). The underlying physical principle of the rotational invariance of the vortex dipole and of its neutrality clearly suggest the presence of a vanishing eigenfrequency pair. We should note here that we have confirmed that higher accuracy (smaller grid spacing) computations reduce the magnitude of the relevant eigenvalues, although their convergence to zero is slow. A more detailed computational investigation of this effect and its convergence to the physically relevant and symmetry mandated zero eigenvalue pair, while worthwhile in its own right is outside the scope of the present manuscript. Thus, we conclude that the sole genuinely unstable mode is due to the relevant eigenfrequency collisions and occurs over a narrow parametric regime.

D. The vortex tripole state

The case of the vortex tripole is illustrated in Fig. 6. The top panel of the figure shows the density and the phase of this three vortex state for $\mu = 3$. The vortices are oriented along a line with adjacent vortices having opposite vorticity. The bottom panel shows the BdG spectrum for $\mu > 0.98$ (where the three vortex state bifurcates into existence).

The real part of the spectrum looks similar to the case of the vortex dipole. However, in this case, the anomalous mode decreasing from the dipolar one and the mode departing from zero cross without creating an oscillatory instability.

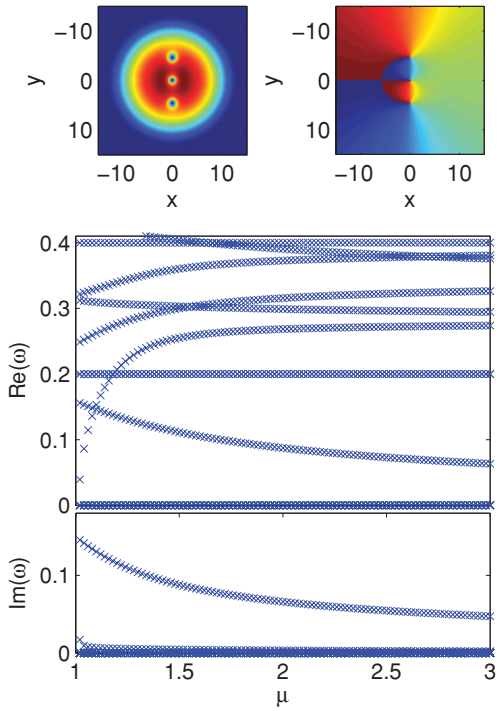

FIG. 6. (Color online) The three-vortex state for a trap strength $\Omega = 0.2$. The top panels show contour plots of the density (left) and phase (right) of the wave function for $\mu = 3$, while the bottom panel shows the eigenfrequencies ω (real and imaginary parts) of the BdG spectrum as a function of the chemical potential μ.

The spectrum contains two zero modes, as in the case of the vortex dipole. The one among them which is (numerically) very weakly nonzero is due to the rotational invariance of the tripole and the corresponding neutrality of this equilibrium (cf. the relevant discussion here and also the discussion of Ref. [24] about the second instability mode therein). Furthermore, as argued earlier on the basis of the general bifurcation approach to this problem, there is always a purely imaginary mode. The magnitude of the purely imaginary mode is comparable to the magnitude of the trap frequency showing that the state is highly unstable, as it inherits the already strong instability of the dark soliton stripe at the chemical potential value where the tripole arises. This is consonant with the discussion of Ref. [24] about a "dominating mode which is roughly an order of magnitude larger" than the other one.

One can extend the vortex particle approach described in Sec. III B to the three-vortex state by adding the corresponding interaction terms. The Jacobian matrix of the linearization around the equilibrium positions of the vortex tripole leads to the following eigenmodes. One of the modes has a vanishing eigenfrequency, similar to the case of the vortex dipole state, corresponding to the "rotational freedom" of the vortex tripole state. Of the other two pairs of eigenmodes, one is real and one is imaginary with respective eigenfrequencies

$$\omega_{\mathrm{pr1}}^{3\mathrm{v}} = \pm\sqrt{5}\omega_{\mathrm{pr}}, \tag{16}$$

$$\omega_{\mathrm{pr2}}^{3\mathrm{v}} = \pm i\sqrt{7}\omega_{\mathrm{pr}}. \tag{17}$$

The former corresponds to the anomalous mode leading to an oscillation of the vortices around their equilibrium positions, and the latter corresponds to the imaginary mode inducing the instability of the system. The modes agree qualitatively with our numerical findings.

The instability of the tripole does not involve the annihilation of a vortex-antivortex pair. Instead, it involves the drift of one of the outer vortices toward the boundary leading to the formation of—essentially—a stable vortex dipole and an outside drifting vortex; see also the relevant discussion of Ref. [24]. The eigenvector of the BdG mode corresponding to the imaginary eigenvalue reflects this tendency as well, as is shown in Fig. 11. An investigation of the eigenvector corresponding to the eigenvalue (17) shows that a similar behavior is predicted by the vortex particle picture.

It is interesting to make some relevant connections here with the recent experimental observations reported in Ref. [53]. In the that work, different types of three-vortex configurations were created, over a large number of realizations of the experimental protocol of excitation of the BEC under an external quadrupolar magnetic field. The principal states observed were an equilateral triangle of same-charge vortices and the previously considered tripole vortex state. For the latter, it was mentioned that it is likely metastable and was observed to decay over long time scales. It was also implied that the potential partial observability of the tripole may be related with the cylindrical geometry used in this experiment rather than the pancake one used here. The metastability (but eventual long-term dynamical instability) of the linear tripole is consistent with our observations here (especially for BECs of large number of atoms, as used in Ref. [53] where the relevant instability becomes weak), although of course the issue of the consideration of the cylindrical geometry remains a relevant question for future studies. Furthermore, another question that arises is whether the equilateral triangle, same-charge vortex configuration can emerge as a result of a bifurcation similarly to the dipole, tripole, etc., considered herein. However, this should arise from a fundamentally different state than the rectilinear ones considered here. In that connection, a relevant possibility is to consider bifurcations from other solitonic states, such as, e.g., the ring dark soliton [40–42]. This constitutes an additional interesting topic for future investigations. Furthermore such a state (an equilateral triangle) should be expected to rigidly rotate. This, in turn, suggests the consideration of periodic orbits of vortices that should be expected to exist in the present system. This constitutes another interesting theme in its own right.

E. The aligned quadrupole state

We now briefly turn to the case of four vortices aligned along the nodal line of the former dark soliton stripe. As in previous figures, Fig. 7 shows some of the characteristics of the four-vortex (4v) aligned state. The bottom panel of the figure shows once again the BdG spectrum for $\mu > 1.26$ (where the four-vortex state exists). Naturally, the real part of the spectrum looks similar to the case of the three-vortex state. As in the case of the vortex dipole and tripole, the rotational and gauge invariances account for the two zero modes. On the other hand, for this four-vortex case, there still exists a single negative-energy mode. However, as anticipated from the stability of the dark soliton stripe at the critical point of the four-vortex-line

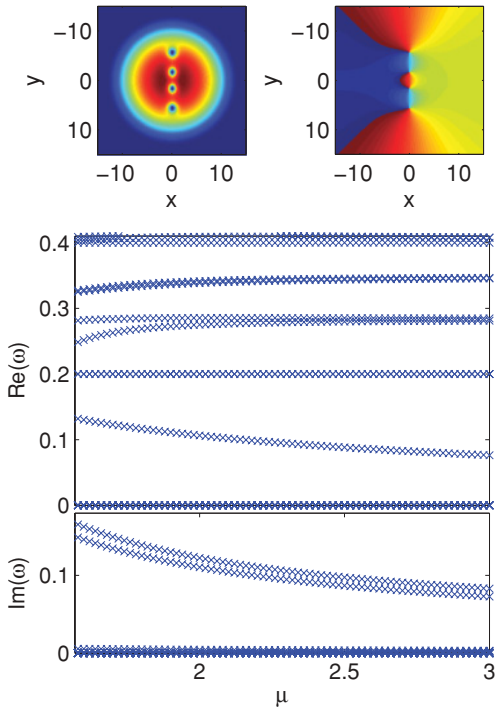

FIG. 7. (Color online) The aligned quadrupole state for a trap strength $\Omega = 0.2$. The top panels show contour plots of the density (left) and phase (right) of the wave function for $\mu = 3$, while the bottom panel shows the (real and imaginary) eigenfrequencies ω of the BdG spectrum as a function of the chemical potential μ.

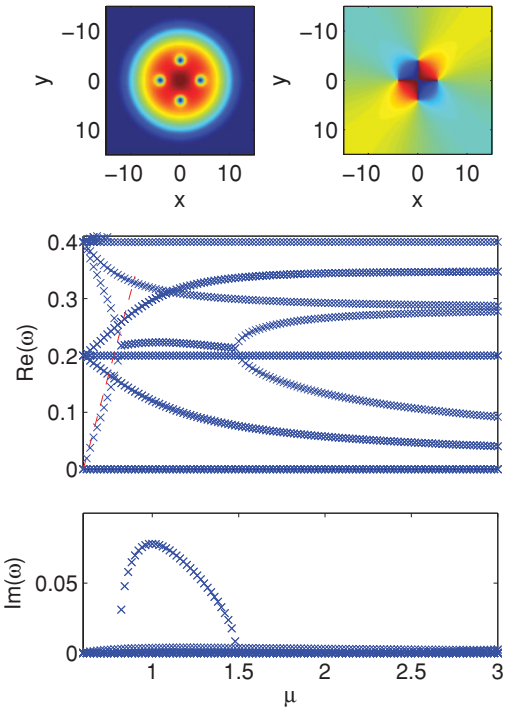

FIG. 8. (Color online) The vortex quadrupole state for a trap strength $\Omega = 0.2$. The top panels show contour plots of the density (left) and phase (right) of the wave function for $\mu = 3$, while the bottom panel shows the (real and imaginary parts of the) eigenfrequencies ω of the BdG spectrum as a function of the chemical potential μ. The dashed line shows the theoretical prediction for the mode departing from zero $\omega = \frac{4\sqrt{2}}{5}(\mu - 3\Omega)$.

bifurcation, in this case there exist two purely imaginary eigenfrequencies in the spectrum. The magnitude of the two purely imaginary modes is comparable to the magnitude of the trap frequency showing that the state is highly unstable, similarly to its dark soliton stripe ancestor in this parametric regime.

It is interesting to observe the count of (stable and) unstable eigenfrequencies of the vortex system in connection to the vortex "particles" participating in the respective state. In the case of two vortices, the epicyclic precession and the vanishing rotational eigenmode accounted for the two modes of the two-particle system. In the case of the tripole, we expect three modes out of the three pairs of ODEs, one of which accounts for the remnant of the epicycles, one for the rotational invariance and one for the mode instability (associated with the outward drift of the outermost vortices toward the condensate boundary). In the aligned quadrupole, there are four modes: the epicycle, the neutral, and the two unstable eigenmodes. For five aligned vortices (see the following), there exist three unstable modes, and so on. As another interesting aside, we note that in none of the earlier studies of Refs. [22–24,26] does this aligned quadrupole state seem to be noted (although, as discussed earlier, its quadrupolar analog was illustrated in Refs. [23,24,64]). However, higher order (such as five and six vortices aligned) were discussed in the anisotropic trap setting also involving rotation in Ref. [31].

F. The vortex quadrupole state

We now make a brief interlude to discuss the quadrupole vortex state of Fig. 8, previously identified in Refs. [23,24,64], again for completeness, although it does not structurally collide with or bifurcate from the dark soliton stripe (instead, as argued here, it emerges from the linear limit). Figure 8 shows density and phase plots of such a state. The bottom panel shows the real and imaginary eigenfrequencies of the BdG spectrum of the quadrupole state as a function of the chemical potential. At $\omega = \Omega$ and $\omega = 2\Omega$ one finds the dipolar and quadrupole modes representing oscillations of the whole condensate. For the vortex quadrupole, negative-energy modes bifurcate from both of these locations. The one departing from the dipolar mode is twofold degenerate, crosses the mode departing from zero, and thus becomes the lowest excitation of the state. The mode departing from the quadrupole limit collides with the mode departing from zero and thus forms an instability band associated with eigenfrequency quartets, as illustrated in the middle and bottom panels of Fig. 8. For larger chemical potentials, this degeneracy is lifted and the negative-energy mode crosses the dipolar mode and becomes the second smallest excitation frequency of the state. Similar to the single-vortex state one can predict the behavior of the mode departing from zero using a small parameter expansion as described in Sec. V B of Ref. [67] yielding

$$\omega = \sqrt{2}(\mu - 3\Omega)\sqrt{\frac{C - D}{C + D}}, \tag{18}$$

with the overlap integrals of the one-dimensional harmonic oscillator eigenfunctions $C = \int dx \psi_0(x)^4 \int dx \psi_2(x)^4$ and

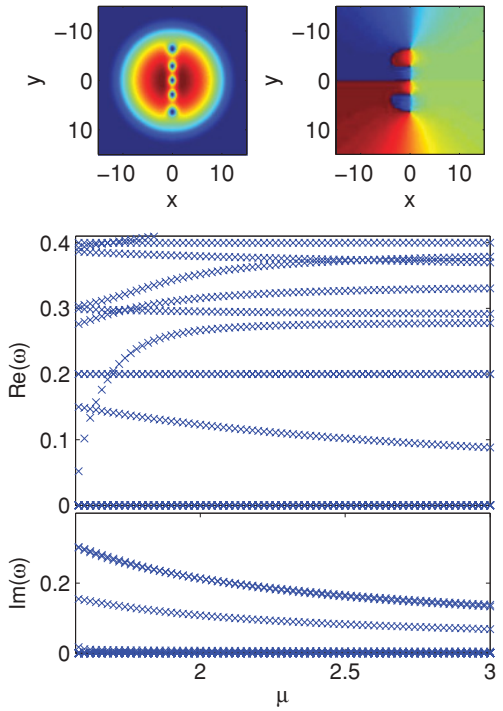

FIG. 9. (Color online) The five-vortex state for a trap strength $\Omega = 0.2$. The top panels show contour plots of the density (left) and phase (right) of the wave function for $\mu = 3$, while the bottom panel shows the real and imaginary parts of the eigenfrequencies ω of the BdG spectrum as a function of the chemical potential μ.

$D = [\int dx \psi_0(x)^2 \psi_2(x)^2]^2$. Evaluation of the integrals yields

$$\omega = \frac{4\sqrt{2}}{5}(\mu - 3\Omega), \tag{19}$$

which is found to be in good agreement with the corresponding numerical result (see dashed line in the real BdG spectrum of Fig. 8).

G. The vortex quintopole state

Last, we briefly mention the five-vortex state in Fig. 9. The presentation of the mode is similar to the earlier ones, with density and phase of a typical representative of this family of solutions being shown in the top panel and real and imaginary eigenfrequencies being demonstrated in the middle and bottom panels. The spectrum looks similar to the spectrum of the earlier states, but as argued earlier, it possesses three purely imaginary eigenfrequencies with two of them being essentially degenerate, as is illustrated in the bottom panel of Fig. 9. Of course, once again the large magnitude of the corresponding eigenfrequencies illustrates the strong dynamical instability of the pertinent structure.

V. VORTEX DYNAMICS: NUMERICAL RESULTS

A. Microscopic displacements

In this section we show results obtained by direct numerical integration of Eq. (1), using as initial conditions stationary states perturbed along the direction of eigenvectors associated with particular eigenfrequencies. Since we are interested in the dynamics of the position of the vortex center we choose eigenfrequencies associated with instabilities or negative-Krein-sign eigenmodes. We should recall at this point that anomalous modes are connected to the oscillation frequencies of the vortices therefore a perturbation along the direction of an eigenvector associated to an anomalous mode leads to a precessional motion of the vortices. In order to determine the position of the vortex as a function of time we first compute the fluid velocity (see, e.g., Ref. [68])

$$\mathbf{v}_s = -\frac{i}{2}\frac{u^*\nabla u - u\nabla u^*}{|u|^2}. \tag{20}$$

The fluid vorticity is then defined as $\omega_{\rm vor} = \nabla \times \mathbf{v}_s$. Due to our setup, the direction of the fluid vorticity is always the z direction and, therefore, we can treat this quantity as a scalar. For well-separated vortices, each vortex leads to a maximum of the absolute value of the fluid vorticity at its location. This allows us to determine the position of the vortices by determining the maxima of the absolute value of the fluid vorticity $\omega_{\rm vor}$. Note the advantages of this definition over alternative techniques such as those discussed in Ref. [26] which attempt to deal with phases and identifying plaquettes of 2π windings. This is evident in the figures illustrated in the following in comparison to the coarse features observed in Figs. 7 and 8 of Ref. [26] (although different grid spacings may be partially responsible too for such differences between our simulations and those of Ref. [26]).

The top panel of Fig. 10 shows the time evolution of the center of the vortices when the vortex dipole state is perturbed

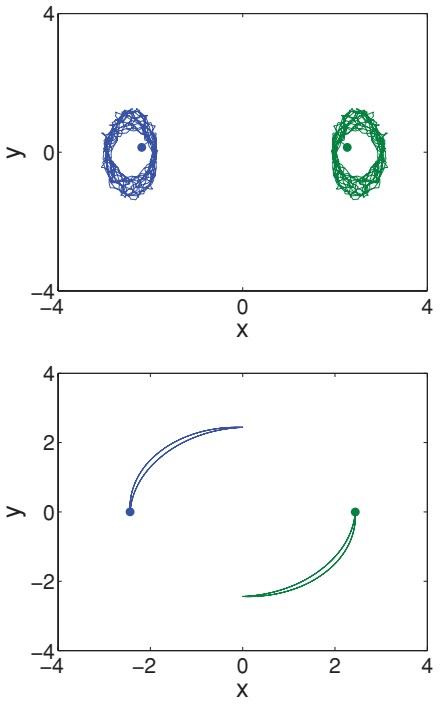

FIG. 10. (Color online) Time evolution of the center of the vortices for the two-vortex state perturbed by the eigenvector of the anomalous mode (top panel) and the eigenvector associated to the zero eigenvalue connected to the rotational invariance (bottom panel) at $\mu = 1.5$. The filled circles represent the initial positions of the vortices.

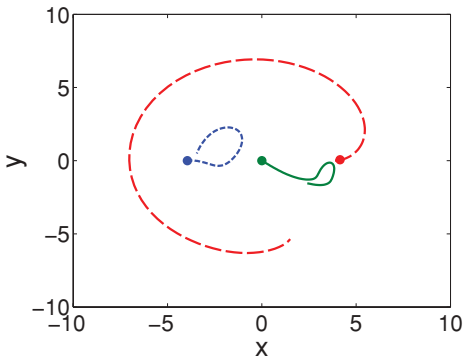

FIG. 11. (Color online) Time evolution of the center of the vortices for the three-vortex state perturbed by the eigenvector of the purely imaginary mode at $\mu = 2.0$. The initial positions of the vortices are depicted by the filled circles.

by the eigenvector corresponding to the anomalous mode for $\mu = 1.5$. Both vortices are initially shifted in the x direction from the equilibrium position toward the center of the trap and in the y direction both were shifted in the same direction namely in the positive half plane. So the vortices are still equidistant from the center of the trap leading to the same value of the background density. During the time evolution the vortices perform an epicyclic (counter-rotating) motion around their respective equilibrium points.

The bottom panel shows the time evolution of the centers of the vortices for the state being perturbed by the eigenvector associated to the (near-) vanishing eigenfrequency corresponding to the rotational invariance at $\mu = 1.5$. Both vortices are displaced symmetrically from the fixed points in such a way that the distance to the origin and the distance between the vortices remains constant. Subsequently they rotate around the center of the trap. After a rotation of $\phi = \pi/2$ they rotate backward. The forward and backward trajectories deviate slightly; yet, despite that, the trajectories are closed. One of the vortices rotates forward on the outer and the other on the inner trajectory and backward vice versa.

In the case of the three-vortex state, on the other hand, there exists an imaginary eigenfrequency mode. Hence, we expect a dynamical manifestation of this strong instability. Figure 11 shows the time evolution of the center of the vortices for the vortex tripole being perturbed by the eigenvector of the imaginary eigenfrequency mode. One of the vortices immediately moves toward the outer regions of the background density (cf. with the corresponding dynamical description of Ref. [24]). The negative-energy and anomalous modes of the states with the vortices oriented along a line lead to similar dynamical evolutions as the corresponding cases discussed here. As an aside, we note that among the rest of the considered states, the one containing a higher multiplicity of anomalous modes is the vortex quadrupole. The twofold degenerate mode with smaller magnitude leads to an in-phase precession of adjacent vortices around the fixed points, whereas the anomalous mode with larger magnitude leads to an out-of-phase precession of the adjacent vortices.

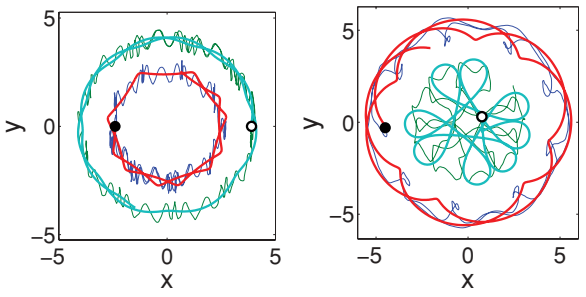

FIG. 12. (Color online) Time evolution of the centers of two vortices for a vortex with positive vorticity and one with negative vorticity initially placed at $(x_0, y_0) = (3.9, 0)$ (white circle) and $(x_0, y_0) = (-2.4, 0)$ (black circle), respectively (left panel), and $(x_0, y_0) = (0.75, 0.3)$ (white circle) and $(x_0, y_0) = (-4.5, -0.3)$ (black circle), respectively (right panel), for $\mu = 3$. The thick solid lines depict the predictions of Eqs. (11) and (12) and the thin solid lines the predictions of Eq. (1).

B. Macroscopic displacements

In this section we show the dynamical evolution of vortices placed at different initial positions and compare the results obtained by direct time integration of Eq. (2) with the results obtained by integrating the corresponding ODEs. We will restrict the investigation in this subsection to two vortices with different vorticities since higher vortex states are unstable. In order to place a vortex at a certain point we use the following procedure. We define the pure vortex wave function as quotient of the single-vortex state in a trap and the background density profile. This pure vortex wave function is then placed at the corresponding point. This procedure excites the background density as well, leading to a small amplitude oscillation of the vortices around a trajectory with large amplitude and frequency. We checked that random numerical noise is not responsible for these fluctuations.

The left panel of Fig. 12 shows the time evolution of two vortices initially placed at $(x_0, y_0) = (3.9, 0)$ (white circle) and $(x_0, y_0) = (-2.4, 0)$ (black circle), respectively. The vortices oscillate around the center of the trap with an approximately constant distance to the trap center. The thick solid lines denote the predictions of Eqs. (11) and (12). They agree very well with the trajectories obtained by integrating Eq. (1) (depicted by thin solid lines). However, the latter results perform an additional small amplitude oscillation due to the excitation of the background condensate as explained earlier. The right panel of Fig. 12 shows the time evolution for vortices initially placed at $(x_0, y_0) = (0.75, 0.3)$ (white circle) and $(x_0, y_0) = (-4.5, -0.3)$ (black circle), respectively. Due to the nonzero displacement in the y direction one does not obtain an oscillation with constant amplitude around the origin but more complicated trajectories of the vortices with varying distances to the trap center. However, the trajectories of the vortices are well separated, i.e., they do not cross. The predictions of Eqs. (11) and (12) (thick solid lines) agree qualitatively well with the corresponding results of the PDE (1) (thin solid lines); however, the oscillation frequency deviates due to the dependence of the integration constants (A, B) on the position of the vortices. The left panel of Fig. 13 shows the evolution for $(x_0, y_0) = (4.5, 0)$ (white circle) and $(x_0, y_0) = (-4.5, 0)$

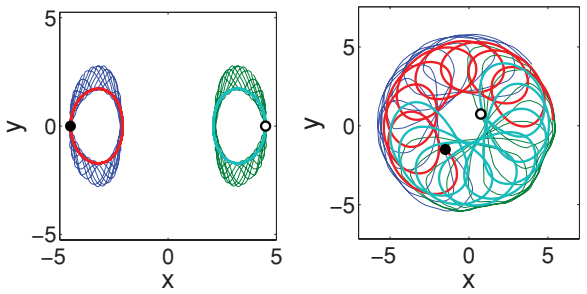

FIG. 13. (Color online) Time evolution of the center of two vortices for a vortex with positive vorticity and one with negative vorticity initially placed at $(x_0, y_0) = (4.5, 0)$ (white circle) and $(x_0, y_0) = (-4.5, 0)$ (black circle), respectively (left panel), and $(x_0, y_0) = (0.75, 0.75)$ (white circle) and $(x_0, y_0) = (-1.5, -1.5)$ (black circle), respectively (right panel), for $\mu = 3$. The thick solid lines depict the predictions of Eqs. (11) and (12) and the thin solid lines the predictions of Eq. (1).

(black circle). Due to the symmetrical displacement of the vortices with respect to the center of the trap, they perform oscillations around their fixed points. The right panel of Fig. 13 shows the evolution for $(x_0, y_0) = (0.75, 0.75)$ (white circle) and $(x_0, y_0) = (-1.5, -1.5)$ (black circle). Both vortices are shifted with respect to their fixed points toward the center of the trap. They perform complicated oscillations around the center of the trap. Once again the qualitative agreement of the prediction by the ODE (11) and (12) is good; however, the exact oscillation frequency cannot be predicted.

In conclusion the trajectories of the two vortices depend strongly on the initial conditions. The qualitative predictions by the ODE agree remarkably well with the PDE results; however, they cannot predict the exact oscillation frequencies. Here, we have attempted to explore, at both the PDE and ODE level, some of the salient features of such "choreographies," as associated with instability and anomalous or invariant modes of the system. Clearly, a more detailed investigation of the possible orbits is warranted and will be forthcoming.

VI. CONCLUSIONS

In this work, we have considered the existence, stability and dynamics of states associated with a dark soliton stripe, as well as of a few related states such as the single vortex and vortex quadrupole, although the latter are not directly related to the solitonic stripe. We have unveiled a systematic cascade of bifurcations from the former state into aligned vortex clusters (or crystals). The symmetry-breaking, supercritical pitchfork nature of the bifurcations was elucidated and a few-mode expansion was employed to identify the corresponding critical points. Although satisfactory approximations to the first four bifurcations were given, the approach is especially successful in the vicinity of the linear limit (and the bifurcation of the vortex dipole state). A complementary viewpoint was also formulated based on a particle picture enabling the development of an ordinary differential equation framework for the evolution of the vortex centers. This approach not only allowed the identification of the equilibrium positions of the vortex clusters but also assisted in the formulation of the vortex linearization problem and the analytical approximation of the vortex epicyclic near-equilibrium motions (e.g., for the vortex dipole), as well as that of the unstable eigenmodes of states such as the tripole. These results were systematically corroborated by existence and numerical linear stability techniques offering good agreement between the analytical approximations and the numerical findings in the relevant regimes.

These results constitute a generalization of both the bifurcation but also, importantly, the particle methods revealed in the realm of one-dimensional dark solitons. This illustrates the strengths of the relevant methodology and suggests various interesting tests, examining its potential generalizations. For example, it could be considered whether similar types of bifurcations may arise from states like the two-dark soliton stripe, i.e., Ψ_{20} (in conjunction with higher order modes with perpendicular nodal lines to it), and whether these could lead to more complicated vortex clusters than the ones discussed here. On the other hand, the relevant considerations are by no means necessarily restricted to the two-dimensional realm. Computational capabilities are on the verge of enabling similar expensive yet tractable bifurcation calculations in three-dimensional settings (associated with bifurcations of vortex rings, etc.). Exploring such generalizations of the present framework and phenomenology would be an exciting direction for future research.

ACKNOWLEDGMENTS

P.G.K. gratefully acknowledges support from NSF-DMS-0349023 (CAREER), NSF-DMS-0806762, and the Alexander von Humboldt Foundation. The work of D.J.F. was partially supported by the Special Account for Research Grants of the University of Athens. R.C.G. gratefully acknowledges the hospitality of Grupo de Física No Lineal (GFNL) of Universidad de Sevilla and support from NSF-DMS-0806762, Plan Propio de la University de Sevilla, Grant IAC09-I-4669 of Junta de Andalucía, and Grant SAB2009-0012 of Ministerio de Educación y Ciencia de España. The authors are also especially grateful to David Hall for numerous constructive discussions and for sharing the results and preprint of Ref. [52].

[1] L. P. Pitaevskii and S. Stringari, *Bose-Einstein Condensation* (Oxford University Press, Oxford, 2003).

[2] C. J. Pethick and H. Smith, *Bose-Einstein Condensation in Dilute Gases* (Cambridge University Press, Cambridge, UK, 2002).

[3] P. G. Kevrekidis, D. J. Frantzeskakis, and R. Carretero-González, *Emergent Nonlinear Phenomena in Bose-Einstein Condensates* (Springer-Verlag, Berlin, 2008).

[4] A. L. Fetter and A. A. Svidzinksy, J. Phys.: Cond. Matt. **13**, R135 (2001).

[5] P. G. Kevrekidis, R. Carretero-González, D. J. Frantzeskakis, and I. G. Kevrekidis, Mod. Phys. Lett. B **18**, 1481 (2004).

[6] R. Carretero-González, P. G. Kevrekidis, and D. J. Frantzeskakis, Nonlinearity **21**, R139 (2008).

[7] Yu. S. Kivshar, J. Christou, V. Tikhonenko, B. Luther-Davies, and L. M. Pismen, Opt. Commun. **152**, 198 (1998).

[8] A. Dreischuh, S. Chevrenkov, D. Neshev, G. G. Paulus, and H. Walther, J. Opt. Soc. Am. B **19**, 550 (2002).

[9] Yu. S. Kivshar and B. Luther-Davies, Phys. Rep. **298**, 81 (1998).

[10] A. S. Desyatnikov, Yu. S. Kivshar, and L. Torner, Prog. Opt. **47**, 291 (2005).

[11] L. M. Pismen, *Vortices in Nonlinear Fields* (Oxford Science, Oxford, UK, 1999).

[12] M. R. Matthews, B. P. Anderson, P. C. Haljan, D. S. Hall, C. E. Wieman, and E. A. Cornell, Phys. Rev. Lett. **83**, 2498 (1999).

[13] J. E. Williams and M. J. Holland, Nature (London) **401**, 568 (1999).

[14] K. W. Madison, F. Chevy, W. Wohlleben, and J. Dalibard, Phys. Rev. Lett. **84**, 806 (2000).

[15] A. Recati, F. Zambelli, and S. Stringari, Phys. Rev. Lett. **86**, 377 (2001).

[16] S. Sinha and Y. Castin, Phys. Rev. Lett. **87**, 190402 (2001).

[17] K. W. Madison, F. Chevy, V. Bretin, and J. Dalibard, Phys. Rev. Lett. **86**, 4443 (2001).

[18] C. Raman, J. R. Abo-Shaeer, J. M. Vogels, K. Xu, and W. Ketterle, Phys. Rev. Lett. **87**, 210402 (2001).

[19] R. Onofrio, C. Raman, J. M. Vogels, J. R. Abo-Shaeer, A. P. Chikkatur, and W. Ketterle, Phys. Rev. Lett. **85**, 2228 (2000).

[20] D. R. Scherer, C. N. Weiler, T. W. Neely, and B. P. Anderson, Phys. Rev. Lett. **98**, 110402 (2007).

[21] A. E. Leanhardt, A. Görlitz, A. P. Chikkatur, D. Kielpinski, Y. Shin, D. E. Pritchard, and W. Ketterle, Phys. Rev. Lett. **89**, 190403 (2002); Y. Shin, M. Saba, M. Vengalattore, T. A. Pasquini, C. Sanner, A. E. Leanhardt, M. Prentiss, D. E. Pritchard, and W. Ketterle, *ibid.* **93**, 160406 (2004).

[22] L.-C. Crasovan, V. Vekslerchik, V. M. Pérez-García, J. P. Torres, D. Mihalache, and L. Torner, Phys. Rev. A **68**, 063609 (2003).

[23] M. Möttönen, S. M. M. Virtanen, T. Isoshima, and M. M. Salomaa, Phys. Rev. A **71**, 033626 (2005).

[24] V. Pietilä, M. Möttönen, T. Isoshima, J. A. M. Huhtamäki, and S. M. M. Virtanen, Phys. Rev. A **74**, 023603 (2006).

[25] A. Klein, D. Jaksch, Y. Zhang, and W. Bao, Phys. Rev. A **76**, 043602 (2007).

[26] W. Li, M. Haque, and S. Komineas, Phys. Rev. A **77**, 053610 (2008).

[27] J.-P. Martikainen, K.-A. Suominen, L. Santos, T. Schulte, and A. Sanpera, Phys. Rev. A **64**, 063602 (2001).

[28] T. Schulte, L. Santos, A. Sanpera, and M. Lewenstein, Phys. Rev. A **66**, 033602 (2002).

[29] D. M. Jezek, P. Capuzzi, M. Guilleumas, and R. Mayol, Phys. Rev. A **78**, 053616 (2008).

[30] R. Geurts, M. V. Milosevic, and F. M. Peeters, Phys. Rev. A **78**, 053610 (2008).

[31] S. McEndoo and Th. Busch, Phys. Rev. A **79**, 053616 (2009).

[32] D. J. Frantzeskakis, J. Phys. A **43**, 213001 (2010).

[33] S. Burger, K. Bongs, S. Dettmer, W. Ertmer, K. Sengstock, A. Sanpera, G. V. Shlyapnikov, and M. Lewenstein, Phys. Rev. Lett. **83**, 5198 (1999).

[34] J. Denschlag, J. E. Simsarian, D. L. Feder, C. W. Clark, L. A. Collins, J. Cubizolles, L. Deng, E. W. Hagley, K. Helmerson, W. P. Reinhardt, S. L. Rolston, B. I. Schneider, and W. D. Phillips, Science **287**, 97 (2000).

[35] B. P. Anderson, P. C. Haljan, C. A. Regal, D. L. Feder, L. A. Collins, C. W. Clark, and E. A. Cornell, Phys. Rev. Lett. **86**, 2926 (2001).

[36] E. A. Kuznetsov and S. K. Turitsyn, Zh. Eksp. Teor. Fiz. **94**, 119 (1988) [Sov. Phys. JETP **67**, 1583 (1988)].

[37] D. L. Feder, M. S. Pindzola, L. A. Collins, B. I. Schneider, and C. W. Clark, Phys. Rev. A **62**, 053606 (2000).

[38] V. Tikhonenko, J. Christou, B. Luther-Davies, and Yu. S. Kivshar, Opt. Lett. **21**, 1129 (1996).

[39] A. V. Mamaev, M. Saffman, and A. A. Zozulya, Phys. Rev. Lett. **76**, 2262 (1996).

[40] G. Theocharis, D. J. Frantzeskakis, P. G. Kevrekidis, B. A. Malomed, and Yu. S. Kivshar, Phys. Rev. Lett. **90**, 120403 (2003).

[41] L. D. Carr and C. W. Clark, Phys. Rev. A **74**, 043613 (2006).

[42] G. Herring, L. D. Carr, R. Carretero-González, P. G. Kevrekidis, and D. J. Frantzeskakis, Phys. Rev. A **77**, 023625 (2008).

[43] A. E. Muryshev, H. B. van Linden van den Heuvell, and G. V. Shlyapnikov, Phys. Rev. A **60**, R2665 (1999).

[44] P. G. Kevrekidis, G. Theocharis, D. J. Frantzeskakis, and A. Trombettoni, Phys. Rev. A **70**, 023602 (2004).

[45] Manjun Ma, R. Carretero-González, P. G. Kevrekidis, D. J. Frantzeskakis, and B. A. Malomed, e-print arXiv:1004.3060.

[46] J. Brand and W. P. Reinhardt, Phys. Rev. A **65**, 043612 (2002).

[47] C. Becker, S. Stellmer, P. Soltan-Panahi, S. Dörscher, M. Baumert, E.-M. Richter, J. Kronjäger, K. Bongs, and K. Sengstock, Nat. Phys. **4**, 496 (2008).

[48] S. Stellmer, C. Becker, P. Soltan-Panahi, E.-M. Richter, S. Dörscher, M. Baumert, J. Kronjäger, K. Bongs, and K. Sengstock, Phys. Rev. Lett. **101**, 120406 (2008).

[49] A. Weller, J. P. Ronzheimer, C. Gross, J. Esteve, M. K. Oberthaler, D. J. Frantzeskakis, G. Theocharis, and P. G. Kevrekidis, Phys. Rev. Lett. **101**, 130401 (2008); G. Theocharis, A. Weller, J. P. Ronzheimer, C. Gross, M. K. Oberthaler, P. G. Kevrekidis, and D. J. Frantzeskakis, Phys. Rev. A **81**, 063604 (2010).

[50] M. A. Hoefer, P. Engels, and J. J. Chang, Physica D **238**, 1311 (2009).

[51] T. W. Neely, E. C. Samson, A. S. Bradley, M. J. Davis, and B. P. Anderson, Phys. Rev. Lett. **104**, 160401 (2010).

[52] D. V. Freilich, D. M. Bianchi, A. M. Kaufman, T. K. Langin, and D. S. Hall, submitted.

[53] J. A. Seman, E. A. L. Henn, M. Haque, R. F. Shiozaki, E. R. F. Ramos, M. Caracanhas, P. Castilho, C. Castelo Branco, K. M. F. Magalhães, and V. S. Bagnato, e-print arXiv:0907.1584.

[54] T. W. B. Kibble, J. Phys. A **9**, 1387 (1976); W. H. Zurek, Nature (London) **317**, 505 (1985); Phys. Rep. **276**, 177 (1996).

[55] C. N. Weiler, T. W. Neely, D. R. Scherer, A. S. Bradley, M. J. Davis, and B. P. Anderson, Nature **455**, 948 (2008).

[56] R. S. MacKay, in *Hamiltonian Dynamical Systems*, edited by R. S. MacKay and J. Meiss (Hilger, Bristol, 1987), p. 137.

[57] D. V. Skryabin, Phys. Rev. A **63**, 013602 (2000); Phys. Rev. E **64**, 055601(R) (2001).

[58] S. Middelkamp, P. G. Kevrekidis, D. J. Frantzeskakis, R. Carretero-González, and P. Schmelcher, J. Phys. B **43**, 155303 (2010).

[59] A. J. Chorin and J. E. Marsden, *A Mathematical Introduction to Fluid Mechanics* (Springer-Verlag, New York, 1993).
[60] P. K. Newton and G. Chamoun, SIAM Rev. **51**, 501 (2009).
[61] G. Theocharis, P. G. Kevrekidis, D. J. Frantzeskakis, and P. Schmelcher, Phys. Rev. E **74**, 056608 (2006).
[62] T. Kapitula and P. G. Kevrekidis, Nonlinearity **18**, 2491 (2005).
[63] E. W. Kirr, P. G. Kevrekidis, E. Shlizerman, and M. I. Weinstein, SIAM J. Math. Anal. **40**, 566 (2008).
[64] T. Kapitula, P. G. Kevrekidis, and R. Carretero-González, Physica D **233**, 112 (2007).
[65] M. Coles, D. E. Pelinovsky, and P. G. Kevrekidis, Nonlinearity **23**, 1753 (2010).
[66] C. Lobo and Y. Castin, Phys. Rev. A **72**, 043606 (2005).
[67] T. Kapitula, P. G. Kevrekidis, and D. J. Frantzeskakis, Chaos **18**, 023101 (2008).
[68] B. Jackson, J. F. McCann, and C. S. Adams, Phys. Rev. Lett. **80**, 3903 (1998).